

Mean-Field Learning for Storage Aggregation

Jingguan Liu, *Graduate Student Member, IEEE*, Cong Chen, *Member, IEEE*, Xiaomeng Ai, *Member, IEEE*, Jiakun Fang, *Senior Member, IEEE*, Jinsong Wang, and Jinyu Wen, *Senior Member, IEEE*

Abstract—Distributed energy storage devices can be pooled and coordinated by aggregators to participate in power system operations and market clearings. This requires representing a massive device population as a single, tractable surrogate that is computationally efficient, accurate, and compatible with market participation requirements. However, surrogate identification is challenging due to heterogeneity, nonconvexity, and high dimensionality of storage devices. To address these challenges, this paper develops a mean-field learning framework for storage aggregation. We interpret aggregation as the average behavior of a large storage population and show that, as the population grows, aggregate performance converges to a unique, convex mean-field limit, enabling tractable population-level modeling. This convexity further yields a price-responsive characterization of aggregate storage behavior and allows us to bound the mean-field approximation error. Leveraging these results, we construct a convex surrogate model that approximates the aggregate behavior of large storage populations and can be embedded directly into power system operations and market clearing. Surrogate parameter identification is formulated as an optimization problem using historical market price-response data, and we adopt a gradient-based algorithm for efficient learning procedure. Case studies validate the theoretical findings and demonstrate the effectiveness of the proposed framework in approximation accuracy, data efficiency, and profit outcomes.

Index Terms—Energy storage aggregation, data-driven modeling, mean-field learning, random set.

I. INTRODUCTION

Coordinated control of demand-side distributed energy resources can substantially increase power system flexibility [1]. In particular, distributed energy storage devices—such as home backup batteries [2]—can shift energy over time and are therefore pivotal flexible resources in renewable-dominated power systems. Aggregating these devices enables a storage aggregator to participate in power system operations and wholesale market clearing as a single virtual resource, submitting aggregate parameters such as total energy capacity, charging and discharging limits, and operating costs [3]. Such participation is supported by FERC Order No. 2222 [4], which removes regulatory barriers to pooling distributed energy resources. This coordinated participation enables population-level regulation capabilities and flexible

responses to market signals [5], providing significant benefits for both system operators and the aggregator.

However, encoding massive storage devices into a single aggregator model is computationally challenging due to their large number, heterogeneous technical parameters, and the nonconvexity of individual feasible operating sets. Direct aggregation requires high-dimensional Minkowski sums of device-level feasible sets, which is NP-hard in general. Therefore, an accurate and computationally efficient aggregation model is essential to capture the behavior of a large population of heterogeneous storage devices while remaining compatible with operational and market-clearing requirements. Motivated by this need, we study how to construct a tractable aggregation model that faithfully approximates the collective performance of distributed storage populations.

A. Related Work

Quantifying the aggregate flexibility and cost of large populations of distributed storage is a key challenge for storage aggregators in power system and market operations. The flexibility of each storage device can be represented as a subset of the power space, and the aggregated flexibility corresponds to the Minkowski sum of these sets [6]. By augmenting the power space with an additional cost dimension, the aggregate cost can be viewed as a function of the aggregate power profiles [7]. Although recent studies have proposed tailored algorithms for exact Minkowski-sum computation [8], [9], they typically rely on strong assumptions—such as unidirectional power and lossless charging/discharging—that limit their practical applicability. In general, computing the exact Minkowski sum remains NP-hard for heterogeneous, nonconvex, and high-dimensional storage devices [10].

Consequently, a variety of model-based approximation methods have been developed to obtain tractable surrogates. A common approach is to approximate each device’s flexibility set with a predefined geometric template that is as tight as possible—for example, boxes [11], ellipses [12], zonotopes [13], homothetic polytopes [1], affine polytopes [14], and vertex-hull representations [15]. These templates admit closed-form computation of Minkowski sums, yielding good scalability for large-scale aggregation. Despite their computational appeal, two limitations still remain: (i) device-level modeling is brittle under highly heterogeneous storage parameters, and per-device approximation errors can accumulate at scale, degrading aggregate accuracy; and (ii) efficient approximation requires each device’s flexibility set

This work is under review. (Corresponding authors: Cong Chen; Xiaomeng Ai.)

Jingguan Liu, Xiaomeng Ai, Jiakun Fang, and Jinyu Wen are with the State Key Laboratory of Advanced Electromagnetic Technology, Huazhong University of Science and Technology, Wuhan 430074, China (e-mail: spencerplusmail@foxmail.com; xiaomengai@hust.edu.cn; jfa@hust.edu.cn; jinyu.wen@hust.edu.cn).

Cong Chen is with the Thayer School of Engineering, Dartmouth College, Hanover, NH 03755, USA (e-mail: Cong.Chen@dartmouth.edu).

Jinsong Wang is with HyperStrong Technology Co., LTD, Beijing 100094, China (e-mail: wangjinsong@hyperstrong.com).

to be convex, an assumption often violated by discrete on/off decisions or mutually exclusive charge/discharge constraints.

Beyond the model-based aggregation methods mentioned above, we also note some recent efforts on data-driven aggregation methods using nonlinear Machine Learning models [16]–[18]. These methods directly apply learning techniques but lack theoretical analysis and physical insights into large-scale storage aggregation. Moreover, their benefits may be limited for storage aggregation settings because (i) available historical data are typically insufficient to train such high-capacity models with statistical reliability, and (ii) the nonlinear Machine Learning formulations are often overparameterized and weakly interpretable, which complicates operational deployment and can conflict with existing market rules [3].

To overcome the above limitations, we develop a mean-field learning approach with theoretical guarantees and physical interpretability. We represent a large population of storage devices by a single *mean-field* aggregate that summarizes their empirical average behavior and characterize its asymptotic performance as the fleet size grows, yielding the *mean-field limit* that reveals population-level aggregation structure and provides operational insights. Mean-field limits have been studied in statistics for variational inference [19], in game theory for Nash equilibria [20], and in pricing applications for home energy management [21]. In contrast, this paper focuses on storage flexibility aggregation, which lies outside the scope of these prior works.

B. Main Contributions

This paper proposes a mean-field learning framework to establish *an accurate and computationally efficient aggregation model* for heterogeneous, nonconvex, and high-dimensional storage populations. The main contributions are threefold:

1) **Theoretical Analysis:** To our knowledge, this is the first work that interprets large-scale storage aggregation as the expectation of random sets in a mean-field setting. Under this viewpoint, we show that as the storage population grows, aggregate performance converges to a unique, convex mean-field limit. This limit enables tractable population-level modeling while accommodating heterogeneous and nonconvex individual devices. The resulting convexity further yields a price-responsive characterization of aggregate behavior and provides a bound on the mean-field approximation error.

2) **Aggregation Framework:** Building on the theoretical results, we design a convex surrogate model for storage aggregation that is compatible with standard wholesale market participation requirements. The surrogate's convexity ensures tractability for power system operations and market clearing, without explicitly computing high-dimensional Minkowski sums across a large population of heterogeneous devices. Leveraging this surrogate, we develop a price-responsive learning framework that identifies aggregate storage behavior from historical market price-response data.

3) **Numerical Analysis:** Through numerical case studies, we demonstrate that the storage aggregator can coordinate large populations of devices, yielding a smoothed aggregate flexibility set that mitigates device-level non-convexities. We further show that our framework learns the convex surrogate with high data efficiency and approximation accuracy. Finally, we verify that the learned surrogate faithfully captures the aggregate economic value and profit-seeking behavior of the storage aggregator in power system operations and market clearing.

C. Paper Organization and Notations

The paper is organized as follows. Section II presents the problem formulations. Section III analyzes mean-field performance to gain aggregation insights. Section IV introduces a mean-field learning framework for surrogate identification. Section V presents case studies, and Section VI concludes.

Regarding notations, we use $\mathbb{P}(\cdot)$ to denote a probability measure. For any vector $\mathbf{x} \in \mathbb{R}^n$, $\|\mathbf{x}\|$ denotes the ℓ_2 norm. For any nonempty, compact set $\mathcal{X} \subset \mathbb{R}^n$, we define $\|\mathcal{X}\| := \sup_{\mathbf{x} \in \mathcal{X}} \|\mathbf{x}\|$. We use $\text{Conv}(\cdot)$ and $\mathbb{E}[\cdot]$ to denote the convex hull and the expectation operator, respectively. For sets $\{\mathcal{X}_i \subset \mathbb{R}^n\}_{i=1}^I$, their Minkowski sum is defined as $\bigoplus_{i=1}^I \mathcal{X}_i := \left\{ \mathbf{x} \mid \mathbf{x} = \sum_{i=1}^I \mathbf{x}_i, \mathbf{x}_i \in \mathcal{X}_i \right\} \subset \mathbb{R}^n$. For any function $f : \mathcal{X} \subseteq \mathbb{R}^n \rightarrow \mathbb{R}$ that is continuous and bounded on a nonempty compact domain \mathcal{X} , we define its truncated epigraph as $\text{epi } f := \left\{ [\mathbf{x}^\top, y]^\top \in \mathbb{R}^{n+1} \mid \mathbf{x} \in \mathcal{X}, f(\mathbf{x}) \leq y \leq \max_{\mathbf{x} \in \mathcal{X}} f(\mathbf{x}) \right\}$. The closed Euclidean ball of radius $R \in \mathbb{R}$ centered at $\mathbf{c} \in \mathbb{R}^n$ is $\mathcal{B}(\mathbf{c}, R) := \{\mathbf{x} \mid \|\mathbf{x} - \mathbf{c}\| \leq R\} \subset \mathbb{R}^n$. For nonempty, compact sets $\mathcal{X}_1, \mathcal{X}_2 \subset \mathbb{R}^n$, we measure their similarity using the Hausdorff distance $d_H(\mathcal{X}_1, \mathcal{X}_2) := \inf \{\varepsilon \geq 0 \mid \mathcal{X}_1 \subseteq \mathcal{X}_2 \bigoplus \mathcal{B}(0, \varepsilon), \mathcal{X}_2 \subseteq \mathcal{X}_1 \bigoplus \mathcal{B}(0, \varepsilon)\}$.

II. PROBLEM FORMULATION

In this section, we present the operational model of individual energy storage devices and formulate the mean-field aggregate performance of the storage fleet.

A. Individual Formulation

We first consider a fleet of energy storage devices, indexed by $i = 1, \dots, I$, over discrete time periods $t = 1, \dots, T$ with time-step length Δ . The operating constraints of each storage device are given by

$$e_{i,t} = e_{i,t-1} + \Delta (p_{i,t}^C \eta_i^C - p_{i,t}^D / \eta_i^D), \quad \underline{e}_i \leq e_{i,t} \leq \bar{e}_i, \quad (1a)$$

$$\underline{p}_i u_{i,t}^C \leq p_{i,t}^C \leq \bar{p}_i u_{i,t}^C, \quad \underline{p}_i u_{i,t}^D \leq p_{i,t}^D \leq \bar{p}_i u_{i,t}^D, \quad (1b)$$

$$u_{i,t}^C, u_{i,t}^D \in \{0, 1\}, \quad u_{i,t}^C + u_{i,t}^D \leq 1. \quad (1c)$$

Here, $p_{i,t}^C$ and $p_{i,t}^D$ denote the charging and discharging power, and $e_{i,t}$ denotes the state of charge (SoC). Constraint (1a) captures the SoC dynamics during charging and discharging, with charging efficiency $\eta_i^C \in (0, 1)$ and discharging efficiency $\eta_i^D \in (0, 1)$, and enforces the SoC bounds $[\underline{e}_i, \bar{e}_i]$.

Constraint (1b) limits the charging and discharging power to device-specific minimum and maximum ratings \underline{p}_i and \bar{p}_i , and activates each operating mode through binary variables $u_{i,t}^C$ and $u_{i,t}^D$. Constraint (1c) enforces mutually exclusive operating modes; that is, a storage device cannot charge and discharge simultaneously in the same period. Only $u_{i,t}^C$ and $u_{i,t}^D$ are binary decision variables; other decision variables, $p_{i,t}^C$, $p_{i,t}^D$, and $e_{i,t}$, are continuous.

Let $\mathbf{p}_i^C := [p_{i,1}^C, \dots, p_{i,T}^C]^\top$, $\mathbf{p}_i^D := [p_{i,1}^D, \dots, p_{i,T}^D]^\top$, and $\mathbf{p}_i := [p_{i,1}^C, \dots, p_{i,T}^C, p_{i,1}^D, \dots, p_{i,T}^D]^\top$. We rewrite (1) as the following flexibility set in the power space for each device:

$$\mathcal{P}_i^E := \{\mathbf{p}_i \mid (1a)-(1c) \text{ hold}\} \subset \mathbb{R}^{2T}. \quad (2)$$

Any feasible profile $\mathbf{p}_i \in \mathcal{P}_i^E$ incurs a cost given by the function $C_i^E(\mathbf{p}_i) : \mathbb{R}^{2T} \rightarrow \mathbb{R}$. We assume that C_i^E is continuous and bounded on \mathcal{P}_i^E . Moreover, C_i^E can be decomposed into (i) a price-response term driven by time-varying electricity prices $\lambda \in \mathbb{R}^T$ and (ii) a linear-quadratic disutility term $U_i^E : \mathbb{R}^{2T} \rightarrow \mathbb{R}$, where $\mathbf{q}_i \in \mathbb{R}^{2T}$ is a cost vector and $\mathbf{Q}_i \in \mathbb{R}^{2T \times 2T}$ is a cost matrix. The disutility term can, for example, capture storage degradation costs incurred during operation [22]:

$$C_i^E(\mathbf{p}_i) := \lambda^\top (\mathbf{p}_i^C - \mathbf{p}_i^D) + U_i^E(\mathbf{p}_i), \quad (3)$$

$$U_i^E(\mathbf{p}_i) := \mathbf{q}_i^\top \mathbf{p}_i + \mathbf{p}_i^\top \mathbf{Q}_i \mathbf{p}_i. \quad (4)$$

The parameters of each device, $\underline{p}_i, \bar{p}_i, \underline{e}_i, \bar{e}_i, \eta_i^C, \eta_i^D, \mathbf{q}_i$, and \mathbf{Q}_i , are modeled herein as i.i.d. random variables drawn from a common distribution.* Under this assumption, the device population can be viewed as an i.i.d. sequence of random sets induced by these parameters. This assumption is reasonable for storage devices manufactured under similar technology standards and is crucial for characterizing population-level aggregation properties. The random-set concepts and mean-field analysis are detailed in Section III.

B. Aggregate Formulation

We now turn to the aggregate formulation of the I devices in mean field. The mean-field *aggregate performance* is characterized by an aggregate flexibility set $\mathcal{P}_I^M \subset \mathbb{R}^{2T}$ and an aggregate cost function $C_I^M(\mathbf{p}) : \mathbb{R}^{2T} \rightarrow \mathbb{R}$, where \mathbf{p} denotes the mean-field aggregate power profile:

$$\mathcal{P}_I^M := \frac{1}{I} \bigoplus_{i=1}^I \mathcal{P}_i^E := \left\{ \mathbf{p} \mid \mathbf{p} = \frac{1}{I} \sum_{i=1}^I \mathbf{p}_i, \mathbf{p}_i \in \mathcal{P}_i^E \right\}, \quad (5)$$

$$C_I^M(\mathbf{p}) := \inf_{\{\mathbf{p}_i\}_{i=1}^I} \left\{ \frac{1}{I} \sum_{i=1}^I C_i^E(\mathbf{p}_i) \mid \mathbf{p} = \frac{1}{I} \sum_{i=1}^I \mathbf{p}_i, \mathbf{p}_i \in \mathcal{P}_i^E \right\}, \quad (6)$$

where (6) selects the least-cost combination of individual devices that delivers the aggregate power profile \mathbf{p} .

*Randomness is a modeling abstraction for population heterogeneity: the fleet's parameter set is a single realization from an underlying population distribution and is then fixed. The mean-field results hold for almost every realization, even if the aggregator observes all individual parameters.

However, for heterogeneous, nonconvex, and high-dimensional operational models of storage devices, computing the exact aggregate performance, i.e., \mathcal{P}_I^M and $C_I^M(\mathbf{p})$, is generally NP-hard. Fortunately, as we show Proposition 1 in Section III-B, when the number of storage goes to infinity, i.e., $I \rightarrow \infty$, there exists a unique pair of mean-field limits with convexity, i.e., a convex aggregate flexibility set

$$\mathcal{P}_I^M \xrightarrow[I \rightarrow \infty]{\text{a.s.}} \mathcal{P}^L \text{ in the Hausdorff metric.} \quad (7)$$

and a convex cost function

$$C_I^M(\mathbf{p}) \xrightarrow[I \rightarrow \infty]{\text{a.s.}} C^L(\mathbf{p}). \quad (8)$$

Approximating the population-level unique, convex mean-field limits is much easier than identifying device-level heterogeneous parameters in a large storage fleet. Accordingly, we do not attempt to model each heterogeneous device directly. Instead, we develop a learning framework that identifies a computationally tractable surrogate for the convex mean-field limits. Specifically, the surrogate consists of an approximate flexibility set $\widehat{\mathcal{P}}^L \approx \mathcal{P}^L$ and an approximate cost function $\widehat{C}^L(\mathbf{p}) \approx C^L(\mathbf{p})$.

Figure 1 summarizes these objects and outlines how they are constructed in the subsequent sections. Specifically, we define: (i) the individual storage performance \mathcal{P}_i^E and $C_i^E(\mathbf{p}_i)$ in (2)-(3); (ii) the mean-field aggregate performance \mathcal{P}_I^M and $C_I^M(\mathbf{p})$ in (5)-(6); (iii) the mean-field limit performance \mathcal{P}^L and $C^L(\mathbf{p})$ in (7)-(8); and (iv) the approximate mean-field limit performance $\widehat{\mathcal{P}}^L$ and $\widehat{C}^L(\mathbf{p})$ in (13)-(14). Section II explains the relationship between individual storage performance and mean-field aggregate performance. Section III discusses the existence and convexity of the mean-field limit performance. Section IV presents the learning method to obtain the approximate mean-field limit performance.

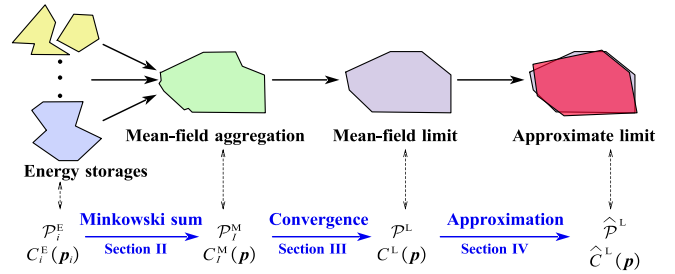


Fig. 1: Conceptual relations across the main sections.

III. MEAN-FIELD PERFORMANCE ANALYSIS

As introduced at the end of Section II-A, we treat the storage population as i.i.d. random sets for our analysis (formalized in Assumption 1 below). In this section, we first review preliminaries on random sets, then theoretically establish the existence and convexity of the mean-field limits for large storage aggregations. Finally, we provide a bound on the mean-field approximation error, which supports the mean-field learning method in Section IV.

A. Preliminaries on Random Sets

To analyze the aggregate performance, we model individual storage devices as random sets and interpret their average Minkowski sums as the expectation of random sets. This viewpoint allows us to invoke law-of-large-numbers-type results for random sets and derive population-level insights when aggregating massive storage devices.

We first recall some basic definitions and a classical lemma as follows. For an intuitive understanding of random sets, Appendix VII-A provides a brief comparison between random variables and random sets. For a comprehensive treatment of random-set theory beyond what is presented here, we refer readers to [23]–[25].

Definition 1 (Random Set [23]). *A random set $\mathcal{X} \subset \mathbb{R}^n$ is a measurable map defined on a probability space and taking values in the family of nonempty, compact subsets of \mathbb{R}^n .*

Definition 2 (Expectation of Random Set [24]). *The Aumann expectation of a random set \mathcal{X} is the set*

$$\mathbb{E}[\mathcal{X}] := \{\mathbb{E}[\mathbf{x}] \mid \mathbf{x} \text{ is a selection of } \mathcal{X}\}.$$

Here, a selection of \mathcal{X} is any random variable $\mathbf{x} \in \mathbb{R}^n$ such that $\mathbf{x} \in \mathcal{X}$ a.s. and \mathbf{x} is integrable, i.e., $\mathbb{E}[\|\mathbf{x}\|] < \infty$; that is, \mathbf{x} almost surely takes values in \mathcal{X} .

Lemma 1 (Strong Law of Large Numbers for Random Sets [25]). *Let $\mathcal{X}_i \subset \mathbb{R}^n, \forall i \in 1, \dots, I$ be i.i.d. random sets defined on a non-atomic probability space and assume that \mathcal{X}_i is integrable, i.e., $\mathbb{E}[\|\mathcal{X}_i\|] < \infty$. Then*

$$\lim_{I \rightarrow \infty} d_H \left(\frac{1}{I} \bigoplus_{i=1}^I \mathcal{X}_i, \mathbb{E}[\text{Conv}(\mathcal{X}_i)] \right) =_{\text{a.s.}} 0,$$

where d_H denotes the Hausdorff distance, $\text{Conv}(\cdot)$ denotes the convex hull operator, and \bigoplus denotes the Minkowski sum.

Lemma 1 is a classical result in random-set analysis, based on the well-known Shapley-Folkman lemma [26]. It connects Minkowski sums to the Aumann expectation of random sets. Intuitively, the average Minkowski sum of an infinite sequence of random sets converges almost surely to the expectation of their convex hulls. This link allows us to characterize the aggregate performance of storage devices via statistical expectation and is the key tool for our mean-field view of storage aggregation.

B. Existence and Convexity of Mean-Field Limits

We now apply Lemma 1 to the storage aggregation problem. We first lift each device's flexibility–cost pair defined in (5) and (6) to an augmented set $\widetilde{\mathcal{P}}_i^E$ in the joint power–cost space by using the truncated epigraph of its cost function, which ensures the compactness of the resulting set. Specifically, for each device i , we define

$$\widetilde{\mathcal{P}}_i^E := \left\{ [\mathbf{p}_i^\top, c_i]^\top \mid \mathbf{p}_i \in \mathcal{P}_i^E, [\mathbf{p}_i^\top, c_i]^\top \in \text{epi } C_i^E \right\} \subset \mathbb{R}^{2T+1}.$$

We then make the following assumption for each device:

Assumption 1 (i.i.d. random sets). *The augmented sets $\widetilde{\mathcal{P}}_i^E, i = 1, \dots, I$, are i.i.d. random sets defined on a non-atomic probability space and satisfy $\mathbb{E}[\|\widetilde{\mathcal{P}}_i^E\|] < \infty$.*

Assumption 1 is practically reasonable in energy storage applications for the following reasons. First, individual devices operate independently, so their performance can be modeled as statistically independent across devices. Second, devices share the same operational architecture, technology standard, and control logic, which makes a common underlying distribution natural. Third, all relevant parameters and state variables are physically bounded, leading to nonempty, compact flexibility sets and bounded costs. These properties ensure that $\widetilde{\mathcal{P}}_i^E$ fall within the scope of Lemma 1.

Recall that the definitions of \mathcal{P}^L and $C^L(\mathbf{p})$ were given in (7) and (8). With Assumption 1, we now establish the existence and convexity of these mean-field limits.

Proposition 1 (Existence and Convexity of Mean-Field Limits). *As the number of storage devices I goes to infinity, the mean-field aggregate flexibility set \mathcal{P}_I^M converges almost surely to a unique nonempty, compact, and convex set, i.e.,*

$$\lim_{I \rightarrow \infty} \mathcal{P}_I^M =_{\text{a.s.}} \mathcal{P}^L, \quad \mathcal{P}^L = \mathbb{E}[\text{Conv}(\widetilde{\mathcal{P}}_i^E)].$$

Also, the mean-field aggregate cost functions $C_I^M(\mathbf{p})$ converge almost surely to a unique function $C^L(\mathbf{p})$ that is convex, continuous, and bounded on the domain \mathcal{P}^L , i.e.,

$$\lim_{I \rightarrow \infty} C_I^M(\mathbf{p}) =_{\text{a.s.}} C^L(\mathbf{p}), \quad \text{epi } C^L(\mathbf{p}) = \mathbb{E}[\text{Conv}(\widetilde{\mathcal{P}}_i^E)].$$

Moreover, $C^L(\mathbf{p})$ admits the decomposition

$$C^L(\mathbf{p}) = \boldsymbol{\lambda}^\top (\mathbf{p}^C - \mathbf{p}^D) + U^L(\mathbf{p}),$$

where $U^L(\mathbf{p})$ is convex, continuous, and bounded on the domain \mathcal{P}^L .

The proof appears in Appendix VII-B. Proposition 1 can be viewed as a variant of Lemma 1, obtained by applying it to the augmented sets introduced above.

Proposition 1 yields two aggregation insights.

(i) *Uniqueness.* Both the aggregate flexibility set and the aggregate cost function admit unique mean-field limits. This enables population-level identification of aggregate performance that accommodates heterogeneous storage parameters.

(ii) *Convexity.* Even when individual flexibility sets and cost functions are nonconvex, the mean-field limit performance is convex. Thus, convex surrogates can be adopted in mean field without sacrificing much approximation accuracy.

However, deriving analytical expressions for the mean-field limits \mathcal{P}^L and $C^L(\mathbf{p})$ is generally intractable. This raises a natural question: *how can we obtain an accurate approximation of these intractable limits for participation in power system operations and market clearing?* To answer this question, we develop a convex surrogate model for aggregated storage and learn its parameters using a price-response approach. This is enabled by the convexity of the mean-field limit, which allows electricity prices to be

interpreted as supporting directions for bounding the set distance in the Hausdorff metric.

In the next subsection, we analyze mean-field approximation error bounds between the ground-truth mean-field limit set \mathcal{A} and the surrogate set \mathcal{B} learned from price-response data. This theoretical result supports the learning framework in Section IV, where the surrogate model formulation and the mean-field learning procedure are presented.

C. Mean-Field Approximation with Price-Response Bounds

Recall from Proposition 1 that the aggregate cost function of the mean-field limit admits the decomposition

$$C^L(\mathbf{p}) = \boldsymbol{\lambda}^\top (\mathbf{p}^C - \mathbf{p}^D) + U^L(\mathbf{p}).$$

Similarly, we design our surrogate cost function as

$$\widehat{C}^L(\mathbf{p}) = \boldsymbol{\lambda}^\top (\mathbf{p}^C - \mathbf{p}^D) + \widehat{U}^L(\mathbf{p}),$$

where \widehat{U}^L denotes a surrogate disutility function that approximates U^L and is convex, continuous, and bounded on its power domain. We then represent the mean-field limit performance in the joint power-disutility space by defining the augmented mean-field limit set

$$\mathcal{A} := \left\{ [\mathbf{p}^\top, u]^\top \mid \mathbf{p} \in \mathcal{P}^L, [\mathbf{p}^\top, u]^\top \in \text{epi } U^L \right\} \subset \mathbb{R}^{2T+1}, \quad (9)$$

and define the corresponding augmented approximate mean-field limit set induced by the surrogate model as

$$\mathcal{B} := \left\{ [\mathbf{p}^\top, u]^\top \mid \mathbf{p} \in \widehat{\mathcal{P}}^L, [\mathbf{p}^\top, u]^\top \in \text{epi } \widehat{U}^L \right\} \subset \mathbb{R}^{2T+1}. \quad (10)$$

To ensure that the surrogate model closely approximates the mean-field limits, our goal is to make set \mathcal{B} as close as possible to set \mathcal{A} . A natural metric for this purpose is the Hausdorff distance $d_H(\mathcal{A}, \mathcal{B})$. However, this distance cannot be evaluated directly because set \mathcal{A} is defined through the intractable limits \mathcal{P}^L and U^L and does not admit an analytical expression. Recognizing this difficulty, we do not work directly with $d_H(\mathcal{A}, \mathcal{B})$. Instead, we analyze their price-response behaviors to construct a tractable upper bound for the set distance $d_H(\mathcal{A}, \mathcal{B})$.

Suppose we observe daily price profiles $\{\boldsymbol{\lambda}_d\}_{d=1}^D$ over D days. For each day d , we define the augmented price vector $\boldsymbol{\pi}_d := [\boldsymbol{\lambda}_d^\top, -\boldsymbol{\lambda}_d^\top, 1]^\top \in \mathbb{R}^{2T+1}$, and collect these vectors in the set $\Pi := \{\boldsymbol{\pi}_d\}_{d=1}^D \subset \mathbb{R}^{2T+1}$. Given a price vector $\boldsymbol{\pi}_d$, the optimal mean-field limit response is defined as

$$[\mathbf{p}_d^{*\top}, u_d^*]^\top \in \arg \min_{[\mathbf{p}^\top, u]^\top \in \mathcal{A}} \boldsymbol{\pi}_d^\top [\mathbf{p}^\top, u]^\top, \quad u_d^* = U^L(\mathbf{p}_d^*),$$

and the corresponding approximate response from our surrogate model is

$$[\widehat{\mathbf{p}}_d^{*\top}, \widehat{u}_d^*]^\top \in \arg \min_{[\mathbf{p}^\top, u]^\top \in \mathcal{B}} \boldsymbol{\pi}_d^\top [\mathbf{p}^\top, u]^\top, \quad \widehat{u}_d^* = \widehat{U}^L(\widehat{\mathbf{p}}_d^*).$$

To quantify how well the price directions in $\Pi := \{\boldsymbol{\pi}_d\}_{d=1}^D$ explore the joint power-disutility space, we use the spherical covering radius

$$\rho(\Pi) := \sup_{\|\mathbf{v}\|=1} \min_{1 \leq d \leq D} \|\mathbf{v} - \boldsymbol{\pi}_d/\|\boldsymbol{\pi}_d\|\|, \quad (11)$$

which measures the worst-case angular distance from a unit vector \mathbf{v} to the normalized price vectors $\boldsymbol{\pi}_d/\|\boldsymbol{\pi}_d\|$.

Also, since \mathcal{A} and \mathcal{B} are nonempty compact subsets of \mathbb{R}^{2T+1} , we can define $R := \|\mathcal{A} \cup \mathcal{B}\| = \sup_{\mathbf{z} \in \mathcal{A} \cup \mathcal{B}} \|\mathbf{z}\|$, which is finite by compactness of $\mathcal{A} \cup \mathcal{B}$.

We can now relate the Hausdorff distance between \mathcal{A} and \mathcal{B} to the observed price-response data.

Proposition 2 (Approximation Error Bound). *Given historical price-response observations $(\boldsymbol{\lambda}_d, \mathbf{p}_d^*, \widehat{\mathbf{p}}_d^*, u_d^*, \widehat{u}_d^*)_{d=1}^D$, we define, for each $d = 1, \dots, D$, the squared error as*

$$e_d^2 := \|\mathbf{p}_d^* - \widehat{\mathbf{p}}_d^*\|^2 + |u_d^* - \widehat{u}_d^*|^2.$$

Then the Hausdorff distance between the mean-field limit set \mathcal{A} in (9) and the approximate mean-field limit set \mathcal{B} in (10) satisfies

$$d_H(\mathcal{A}, \mathcal{B}) \leq 2R \rho(\Pi) + \sqrt{\sum_{d=1}^D e_d^2}.$$

The proof of Proposition 2 is given in Appendix VII-C. Proposition 2 provides two intuitive insights.

(i) *Coverage of price directions.* The set distance is bounded by the spherical covering term $2R \rho(\Pi)$. As the historical price signals $\{\boldsymbol{\pi}_d\}_{d=1}^D$ become more diverse and span more directions in the augmented space, $\rho(\Pi)$ decreases and the bound tightens.

(ii) *Tracking of optimal responses.* The set distance is also controlled by the sum of squared gaps $\sqrt{\sum_{d=1}^D e_d^2}$ between the optimal response profiles across the observed price signals. This highlights the need to design an accurate surrogate model so that its optimal responses closely track the mean-field optimal responses.

Based on Proposition 2, we can control $d_H(\mathcal{A}, \mathcal{B})$ using observable price-response data. For a given collection of historical price directions Π , $\rho(\Pi)$ is fixed and we focus on minimizing the response-tracking term $\sqrt{\sum_{d=1}^D e_d^2}$ by fitting the surrogate such that its optimal responses $(\widehat{\mathbf{p}}_d^*, \widehat{u}_d^*)$ closely match the mean-field optimal responses (\mathbf{p}_d^*, u_d^*) across the observed price signals. This directly motivates the learning objective in (16), as detailed in Section IV-C.

At this point, one question remains: *how can we obtain the optimal response profiles $[\mathbf{p}_d^{*\top}, u_d^*]^\top$ without an analytical expression of the mean-field limit set \mathcal{A} ?* To address this issue, we first represent the device-level performance ((2) and (4)) in the joint power-disutility space by defining

$$C_i := \left\{ [\mathbf{p}_i^\top, u_i]^\top \mid \mathbf{p}_i \in \mathcal{P}_i^E, [\mathbf{p}_i^\top, u_i]^\top \in \text{epi } U_i^E \right\} \subset \mathbb{R}^{2T+1}, \quad (12)$$

where C_i is in the power-disutility space for storage i .

Inspired by [21], we next use the strong law of large numbers to establish the consistency of the optimal responses.

Proposition 3 (Consistence of Optimal Responses). *For any augmented price vector $\boldsymbol{\pi}_d$, the optimal device-level response is defined as*

$$[\mathbf{p}_{i,d}^{*\top}, u_{i,d}^*]^\top \in \arg \min_{[\mathbf{p}^\top, u]^\top \in C_i} \boldsymbol{\pi}_d^\top [\mathbf{p}^\top, u]^\top, \quad u_{i,d}^* = U_i^E(\mathbf{p}_{i,d}^*).$$

Then there exists a mean-field optimal response $[\mathbf{p}_d^{*\top}, u_d^*]^\top$ such that

$$\lim_{I \rightarrow \infty} \frac{1}{I} \sum_{i=1}^I \mathbf{p}_{i,d}^* =_{\text{a.s.}} \mathbf{p}_d^*, \quad \lim_{I \rightarrow \infty} \frac{1}{I} \sum_{i=1}^I u_{i,d}^* =_{\text{a.s.}} u_d^*.$$

The proof of Proposition 3 is given in Appendix VII-D. Proposition 3 shows that the optimal mean-field limit profile can be efficiently recovered from the sample mean over a large storage population, so that the intractable mean-field limits can be approximated from observed device-level responses under given electricity prices. In practice, device-level power responses are often readily available from smart-meter measurements [27]. The device-level disutility cost can be obtained by summing the product of its market-level bid disutility price and its realized response power over time.

With the above theoretical analysis in hand, we now turn to constructing a mean-field learning framework that derives analytical expressions for the surrogate ($\widehat{\mathcal{P}}^L$ and $\widehat{U}^L(\mathbf{p})$) from historical price-response data.

IV. MEAN-FIELD LEARNING FRAMEWORK

In this section, we first outline the learning framework and formulate the surrogate model. We then define an optimization problem to identify the surrogate parameters and present a gradient-based algorithm for efficient learning procedure.

A. Framework Overview

Fig. 2 summarizes the proposed learning framework. Guided by Proposition 1, we first choose a convex, market-compatible surrogate to approximate the mean-field limit, consisting of a convex parameterized cost function \widehat{C} and a convex parameterized set $\widehat{\mathcal{P}}$ for aggregated storage, as shown in green in the left panel of the figure and discussed in Section IV-B. Guided by Proposition 3, we use device-level historical response data to construct mean-field price-response pairs, as shown at the top of the figure. Using the surrogate structure and the historical data as inputs, and building on Proposition 2, we formulate a parameter identification problem that minimizes the discrepancy between the surrogate-based mean-field responses and the observed historical mean-field responses over the dataset, as illustrated in the central black box and discussed in Section IV-C. We solve this problem using a gradient-based algorithm, as shown in the central dashed gray box and discussed in Section IV-D. The identified surrogate model then enables storage aggregators to submit bids that are compatible with power system operations and wholesale market clearing.

B. Surrogate Model for Mean-Field Limit Approximation

Motivated by the market rules and the analysis in Proposition 1, we propose a convex surrogate model to approximate the mean-field limit of the aggregate storage performance [3], [28]. The model is parameterized by

$$\Theta := \{\eta^C, \eta^D, \bar{p}^C, \bar{p}^D, \underline{e}, \bar{e}, \mathbf{q}, \mathbf{Q}\},$$

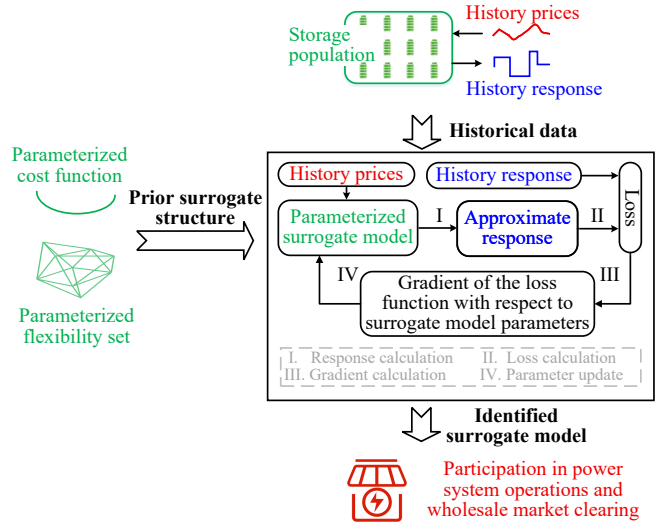


Fig. 2: Flowchart of the proposed learning framework.

where $\mathbf{q} \in \mathbb{R}^{2T}$ is a linear cost vector and $\mathbf{Q} \in \mathbb{R}^{2T \times 2T}$ is a diagonal positive-definite cost matrix. The surrogate consists of a storage-like power space set and a quadratic cost function:

$$\widehat{\mathcal{P}}^L(\Theta) := \left\{ \mathbf{p} \mid \begin{array}{l} 0 \leq p_t^C \leq \bar{p}^C, 0 \leq p_t^D \leq \bar{p}^D, \underline{e} \leq e_t \leq \bar{e}, \\ e_t = e_{t-1} + \Delta(p_t^C \eta^C - p_t^D \eta^D) \end{array} \right\}, \quad (13)$$

$$\widehat{C}^L(\mathbf{p}, \Theta) := \mathbf{\lambda}^\top (\mathbf{p}^C - \mathbf{p}^D) + \widehat{U}^L(\mathbf{p}), \quad \widehat{U}^L(\mathbf{p}) := \mathbf{q}^\top \mathbf{p} + \mathbf{p}^\top \mathbf{Q} \mathbf{p}. \quad (14)$$

The aggregator participates in power system operations and wholesale market clearing using a virtual storage representation, such as the Non-Generator Resource model in CAISO [3]. In this framework, the bidding parameters consist of operational limits and bidding costs. The operational limits are captured by (13), together with the mutually exclusive charging-discharging requirement (15):

$$p_t^C p_t^D = 0, \quad \forall t \in \{1, \dots, T\}, \quad (15)$$

which is automatically enforced by the market operator in the market clearing engine. The bidding cost is modeled as a piecewise-linear approximation of $\widehat{U}^L(\mathbf{p})$ in the surrogate objective (14). Thus, our surrogate is ready for participation in power system operations and wholesale market clearing.

Note that we formulate our surrogate model (13)–(14), intentionally omitting (15) to enable efficient aggregation across heterogeneous storage devices. When market participation reintroduces this exclusivity constraint on top of our surrogate, we observe a further improvement in the accuracy of the surrogate representation (shown in Fig. 3(e)(f)).

C. Parameter Identification for Surrogate Model

Motivated by the analysis in Propositions 2 and 3, we formulate the optimization problem (16), which selects Θ to minimize the loss function F measuring the discrepancy between the surrogate-based mean-field responses and those

observed in the historical dataset. Solving (16) yields surrogate parameters Θ that make the surrogate model \mathcal{B} in (10) closely match the intractable mean-field limit set \mathcal{A} in (9):

$$\begin{aligned} \min_{\Theta} F(\Theta) &:= \frac{1}{D} \sum_{d=1}^D \left(\left\| \hat{\mathbf{p}}_d^* - \frac{1}{I} \sum_{i=1}^I \mathbf{p}_{i,d}^* \right\|^2 + \left| \hat{u}_d^* - \frac{1}{I} \sum_{i=1}^I u_{i,d}^* \right|^2 \right) \\ \text{s.t. } & \left[\hat{\mathbf{p}}_d^{*\top}, \hat{u}_d^* \right]^\top \in \arg \min_{[\mathbf{p}^\top, u]^\top \in \mathcal{B}(\Theta)} \pi_d^\top [\mathbf{p}^\top, u]^\top, \forall d \in \{1, \dots, D\}. \end{aligned} \quad (16)$$

D. Solution Algorithm for Parameter Identification Problem

While natural to state, problem (16) is a large-scale bilevel program and is challenging to solve. Fortunately, the outer level of (16) is an unconstrained optimization over Θ . This structure enables us to leverage recent advances in *differentiable optimization layers* in the machine learning literature [29], [30] and to solve this problem iteratively via gradient-based algorithms. Specifically, we compute the gradient of F w.r.t. Θ and update the surrogate parameters via gradient descent. Define the surrogate optimal response $\mathbf{z}_\mathcal{B}^*(\pi_d) := [\hat{\mathbf{p}}_d^{*\top}, \hat{u}_d^*]^\top$. At iteration o , we update Θ via

$$\Theta^{(o+1)} \leftarrow \Theta^{(o)} - \kappa \sum_{d=1}^D \frac{\partial F^{(o)}}{\partial \mathbf{z}_\mathcal{B}^{*(o)}(\pi_d)} \frac{\partial \mathbf{z}_\mathcal{B}^{*(o)}(\pi_d)}{\partial \Theta^{(o)}}, \quad (17)$$

where κ is the learning rate; $\partial F^{(o)} / \partial \mathbf{z}_\mathcal{B}^{*(o)}(\pi_d)$ is the gradient of the loss w.r.t. the mean-field response and can be computed directly from (16); and $\partial \mathbf{z}_\mathcal{B}^{*(o)}(\pi_d) / \partial \Theta^{(o)}$ captures the sensitivity of the response to the surrogate parameters. The latter term is obtained by differentiating the KKT conditions of the inner problem (18):

$$\min_{\mathbf{z}_\mathcal{B}(\pi_d) \in \mathcal{B}(\Theta)} \pi_d^\top \mathbf{z}_\mathcal{B}(\pi_d). \quad (18)$$

We defer the detailed gradient derivations and algorithmic steps, which follow the standard forward–backward training procedure for differentiable optimization, to Appendix VII-E.

V. CASE STUDIES

In this section, we first use an illustrative toy example to validate the theoretical analysis. We then compare the proposed mean-field learning framework with existing data-driven approaches using price-response data. Finally, we benchmark the proposed surrogate model against existing model-based aggregation approaches under a price-taking assumption in power system operation and market clearing.

A. Simulation Setup

1) *Parameter settings.* We consider an aggregation of $I = 1,000$ energy storage devices with parameters listed in Table I. Each parameter is independently sampled across devices from a uniform distribution $U[\cdot, \cdot]$. The scalar α controls the degree of heterogeneity across devices and is set to $\alpha = 1$ unless otherwise specified. The time step is fixed at $\Delta = 1$ hour. Electricity prices are constructed from

TABLE I: Parameters of energy storage devices.

Item	Value	Unit
\bar{p}_i	$U[15-10\alpha, 15+10\alpha]$	kW
\underline{p}_i	$\bar{p}_i \cdot U[0.2-0.1\alpha, 0.2+0.1\alpha]$	kW
\bar{e}_i	$\bar{p}_i \cdot U[2.5-1.5\alpha, 2.5+1.5\alpha]$	kWh
\underline{e}_i	$\bar{e}_i \cdot U[0.2-0.1\alpha, 0.2+0.1\alpha]$	kWh
η_i^c	$U[0.9-0.1\alpha, 0.9+0.1\alpha]$	/
η_i^d	$U[0.9-0.1\alpha, 0.9+0.1\alpha]$	/
q_i	$U[5-5\alpha, 5+5\alpha]$	\$/MWh
Q_i	$U[5-5\alpha, 5+5\alpha]$	\$/({MWh}^2)

NYISO Zone J hourly locational marginal prices (LMPs) on randomly selected calendar days [31].

2) *Test platform.* All numerical experiments are conducted on a laptop with a 2.20 GHz CPU and 32 GB of RAM. The optimization problems are solved using *Gurobi*. The gradient calculation in (18) is computed in *PyTorch* using differentiable convex optimization layers implemented via *CVXPYLayers* [30].

B. An Illustrative Toy Example

We start with a two-period example ($T = 2$) to visualize the mean-field flexibility set in Fig. 3, and illustrate the impact of the number of price samples and devices in Fig. 4. Define the mean-field net power as $x_t := \frac{1}{I} \sum_i (p_{i,t}^c - p_{i,t}^d)$. For visualization, we plot the exact mean-field aggregate flexibility set by densely sampling feasible operating points in Fig. 3. To generate training data for the surrogate identification, we sample price signals in \mathbb{R}^2 uniformly on the unit circle. Unless otherwise specified, we use $D = 20$ price samples in this toy example.

In Fig. 3(a)–(d), the device number I increases from 1 to 300 and we observe the following behavior for the shape of the feasibility set. For $I = 1$, the individual flexibility set is disconnected and nonconvex due to the integer variables in (1). When $I = 2$, the aggregate set becomes connected and exhibits less pronounced nonconvexity. By $I = 100$, the aggregate set is nearly convex, and for $I = 300$ it is almost indistinguishable from the $I = 100$ case. These patterns are consistent with Proposition 1, which states that the mean-field performance converges to a unique, convex set as I grows. The *cooperative effect* behind this behavior is intuitive: a single storage device cannot charge and discharge at the same time, but a large aggregation can coordinate devices so that some charge while others discharge. This coordinated and complementary operation allows the aggregation to mimic fractional charging and discharging states that individual devices cannot realize, smoothing out discreteness and yielding an approximately convex flexibility set.

Fig. 3(e) compares the aggregate set with the trained surrogate. Overall, the surrogate closely matches the aggregate set,

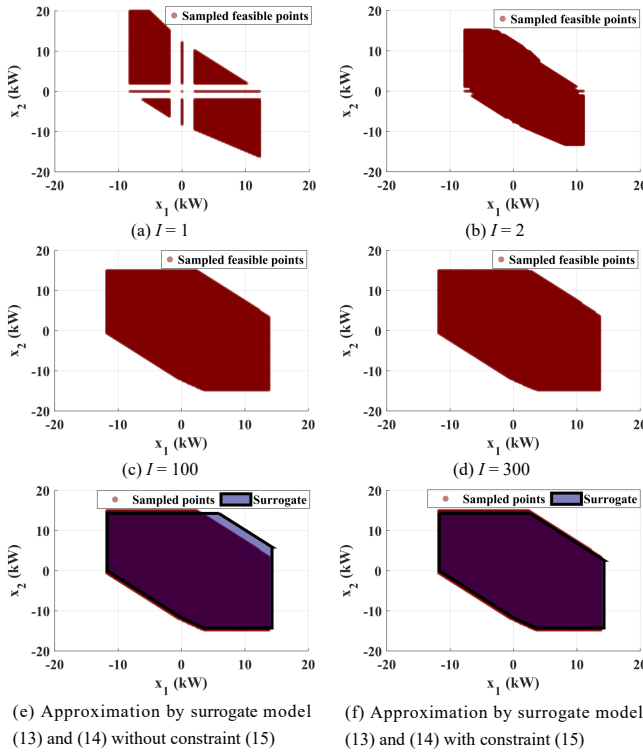


Fig. 3: Visualization of mean-field flexibility set.

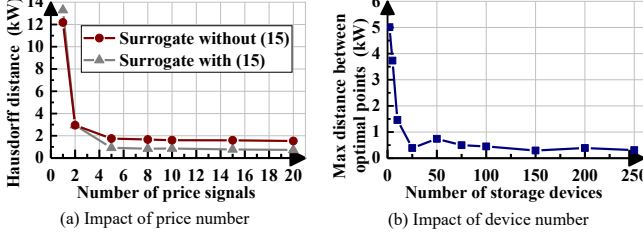


Fig. 4: Impact of price number and device number.

with a small overestimated region in the upper-right corner. This region corresponds to relaxed operating points that allow simultaneous charging and discharging, which are inactive for the surrogate's optimal price response. The overestimation arises because our convex surrogate is trained from historical optimal power profiles, rather than from the full flexibility set of problem (18). In practice, when the aggregator submits the surrogate to the wholesale market, the market-clearing model enforces the constraint (15) for the represented resource [3], which removes this invalid relaxed region at the top right of Fig. 3(e). The resulting flexibility set, shown in Fig. 3(f), then almost coincides with the exact aggregate flexibility set. This observation validates the effectiveness of our mean-field learning framework.

Fig. 4(a) further compares the Hausdorff distance between the trained surrogate and the exact aggregate set under different numbers of sampled prices. As the price information

becomes richer, more optimal-solution information is incorporated into training. As a result, this set distance decreases, indicating that the surrogate approaches the exact aggregate set more closely. This observation supports Proposition 2. Fig. 4(b) shows that, as the number of storage devices increases, the maximum distance (over $D = 20$ test price signals) between (i) the sample mean of device-level optimal solutions and (ii) the mean-field optimal solution computed from the aggregate set with $I = 300$ decreases. This trend suggests that sampling device-level optimal solutions increasingly approximates the mean-field optimum. This observation supports Proposition 3.

Overall, this toy example intuitively illustrates our theoretical analysis and validates the effectiveness of the proposed mean-field learning framework.

C. Validation of Mean-Field Learning Framework

We now consider a 24-hour horizon ($T = 24$) to evaluate the proposed learning framework for aggregating $I = 1,000$ storage devices. The approximation accuracy is measured by the per-day normalized root-mean-square error (RMSE) of the response power, i.e., $\|\hat{\mathbf{p}}_d^* - \mathbf{p}_d^*\| / (T \max_t |\mathbf{p}_{d,t}^*|) \times 100\%$. We compare our learning framework with three machine-learning baselines: multilayer perceptron (MLP), support vector regression (SVR), and long short-term memory (LSTM) models. These baselines are implemented in Pytorch and details about the network architecture are provided in Appendix VII-F. Our surrogate model is trained using $D = 30$ daily price samples, since only a small number of parameters need to be learned. The large-capacity baselines use $D = 210$ training samples because their performance degrades markedly with fewer data. Testing is conducted on another 30 days with unseen price realizations. The results are summarized in Fig. 5.

From Fig. 5(a), we observe that, with only 30 days of hourly training data, the proposed learning framework achieves the lowest normalized RMSE on the test set, remaining below 10% for every day. The superior approximation accuracy and data efficiency stem from the convex surrogate model guided by prior insight into the mean-field limit, whose compact parameterization in (13) and (14) captures the essential aggregate performance using only a few physical parameters Θ . As a result, the estimated aggregate power profiles closely track the ground-truth aggregate trajectories, as shown in Fig. 5(b).

In contrast, the three baselines (MLP, SVR, LSTM) exhibit substantially higher RMSEs on the test set, even though they are trained on seven times more data ($D = 210$). Because these models must infer the complex aggregate performance purely from data, without exploiting the underlying physical structure in the mean field setting, they tend to generalize poorly to unseen price patterns and produce aggregate power profiles that visibly deviate from the ground-truth curves.

Overall, these results highlight both the data efficiency and the approximation accuracy of our learning method.

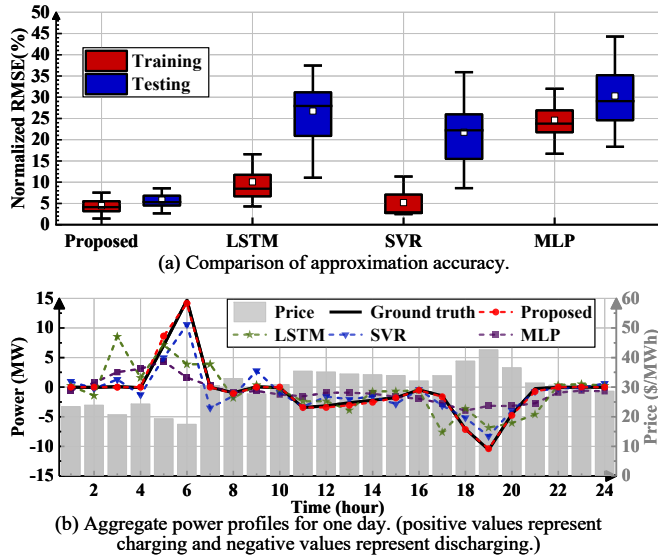


Fig. 5: Learning results of different methods.

D. Simulation as a Price-Taker in Power System Operation and Market Clearing

We next run a one-month power system operation and market clearing simulation in which the storage aggregator is assumed to be a price-taker thus truthfully reports the physical operation limits and cost to the power system operator. In this setting, the surrogate bid does not affect the LMPs λ_d , which are treated as exogenous. Given λ_d , we solve (18) under each aggregation method to obtain the optimal scheduling power curve and the corresponding profit outcome, defined as the negative of the total cost, i.e., the negative value of the objective in (18).

We compare our learning-based aggregation with a state-of-the-art model-based aggregation method[†] [1], [14], which produces a structure-preserving virtual-battery surrogate that satisfies the storage participation model in the power system operation and market clearing. Note that these model-based methods assume that each device admits a convex formulation. To make them applicable to our nonconvex storage model, we relax each device's integer variables to continuous variables in $[0, 1]$.

Market performance is evaluated using a daily profit-gap metric, defined as the daily relative error between (i) the profit earned by the aggregated storage population when bidding through a given aggregation method and (ii) an ideal (but impractical) benchmark in which each device bids individually. A smaller profit gap indicates that the aggregation preserves most of the individual-storage revenue, whereas a large gap may discourage storage owners from joining the aggregation. The market simulation results are summarized in Fig. 6.

[†]We do not include some model-based aggregation methods for comparison, such as ellipsoid-based methods [13], because they violate market bidding requirements and cannot be embedded in power system operations.

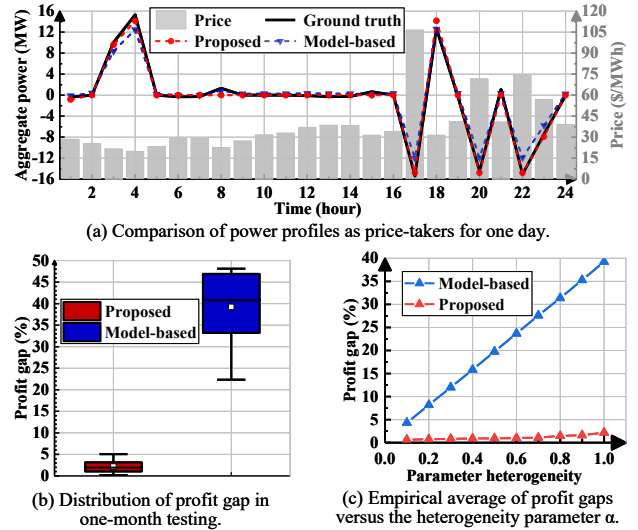


Fig. 6: Simulation results in the wholesale market.

From Fig. 6(a), both the proposed learning-based method and the model-based method capture the overall charging and discharging patterns of the aggregated power. However, the model-based method constructs the surrogate by aggregating approximate device-level models. This device-level construction is brittle under highly heterogeneous storage parameters: small per-device modeling errors can accumulate at scale and degrade aggregate accuracy. Moreover, the physical storage model is inherently nonconvex (e.g., charge-discharge complementarity), while the model-based surrogate typically relies on convexified approximations; this mismatch can further distort the feasible set and cost, leading to a pronounced loss in market performance. As a result, the model-based method exhibits a large performance gap, with an average profit gap close to 40% in Fig. 6(b).

In contrast, our surrogate is learned directly at the population level and is therefore much less sensitive to heterogeneity. It achieves an average profit gap of about 3%, with the maximum remaining below 6%. This improvement is driven by explicitly incorporating historical optimal power schedules and their associated costs into the learning objective (see (16)), which prioritizes accuracy on profit-relevant operating points. In addition, the error distribution of the proposed method in Fig. 6(b) is noticeably more concentrated than that of the model-based approach, indicating more robust market performance across price scenarios. Fig. 6(c) further highlights the role of heterogeneity by reporting the empirical average profit gap as a function of heterogeneity parameter α . As α increases, the profit gap of the model-based method grows rapidly, whereas the proposed method maintains a consistently low profit gap across all heterogeneity levels.

Overall, these results confirm that the learned surrogate faithfully captures the aggregate economic value and profit-seeking behavior of the storage aggregator in power system operations and market clearing.

VI. CONCLUSION

This paper proposes a mean-field learning framework to derive an operational model for an aggregator that coordinates massive heterogeneous storage resources. Motivated by the convexity of mean-field performance, the framework enables power system and electricity market operators to schedule storage aggregators efficiently and accurately. We first interpret storage aggregation as the expectation of random sets and show that the aggregation converges to a unique, convex mean-field limit. We then derive bounds on the mean-field approximation error via a price-response analysis. Building on these results, we leverage historical price-response data to identify an accurate, market-compatible surrogate model for the storage aggregator.

Our theoretical results and numerical experiments demonstrate that (i) the coordinated and complementary operation of a large storage fleet smooths device-level nonconvexities, yielding a unique convex mean-field limit for the storage aggregator; (ii) guided by convex structural insights into the mean-field limit, the proposed framework identifies surrogates with high data efficiency and approximation accuracy; and (iii) identified from population-level price-response data, the learned surrogate faithfully captures both the aggregate economic value and the profit-seeking behavior of the storage aggregator in power system operations and market clearing.

ACKNOWLEDGEMENT

The authors would like to thank Prof. Eilyan Bitar from Cornell University for many insightful discussions. We also thank Dr. Shengshi Wang for helpful comments.

REFERENCES

- [1] J. Liu, X. Ai, S. Cui, X. Xue, S. Wang, J. Fang, W. Yao, and J. Wen, “Preference-oriented aggregation of heterogeneous distributed energy resources for reserve dispatch,” *IEEE Transactions on Smart Grid*, 2025.
- [2] “Texas’ only energy provider with home backup power,” [Online]. Available: <https://www.basepowercompany.com/>, accessed: Nov. 6, 2025.
- [3] “Bid and self-schedule submission in California ISO markets,” [Online]. Available: <https://www.caiso.com/documents/section-30-bid-and-self-schedule-submission-in-california-iso-markets-as-of-aug-1-2024.pdf>, August 2024, accessed: Nov. 6, 2025.
- [4] “FERC order no. 2222: Fact sheet,” [Online]. Available: <https://www.ferc.gov/media/ferc-order-no-2222-fact-sheet>, Sep. 2020, accessed: Nov. 6, 2025.
- [5] Y. Bian, N. Zheng, Y. Zheng, B. Xu, and Y. Shi, “Predicting strategic energy storage behaviors,” *IEEE Transactions on Smart Grid*, vol. 15, no. 2, pp. 1608–1619, 2023.
- [6] J. Liu, H. Jiang, X. Ai, S. Wang, X. Xue, S. Cui, J. Hou, J. Fang, and J. Wen, “Coupling-aware aggregation of multi-zone HVAC loads under uncertainty: A two-level framework,” *IEEE Transactions on Smart Grid*, 2025.
- [7] Z. Long, N. Zhang, K. Feng, Y. Wang, and J. Wang, “Characterizing the flexibility of electric vehicle fleets considering battery degradation cost,” *IEEE Transactions on Industry Applications*, 2025.
- [8] N. K. Panda and S. H. Tindemans, “Efficient quantification and representation of aggregate flexibility in electric vehicles,” *Electric Power Systems Research*, vol. 235, p. 110811, 2024.
- [9] D. Angeli, Z. Dong, and G. Strbac, “Exact aggregate models for optimal management of heterogeneous fleets of storage devices,” *IEEE Transactions on Control of Network Systems*, vol. 11, no. 3, pp. 1430–1439, 2023.
- [10] J. Liu, X. Ai, J. Fang, S. Cui, S. Wang, W. Yao, and J. Wen, “Continuous-time aggregation of massive flexible HVAC loads considering uncertainty for reserve provision in power system dispatch,” *IEEE Transactions on Smart Grid*, vol. 15, no. 5, pp. 4835–4849, 2024.
- [11] X. Chen, E. Dall’Anese, C. Zhao, and N. Li, “Aggregate power flexibility in unbalanced distribution systems,” *IEEE Transactions on Smart Grid*, vol. 11, no. 1, pp. 258–269, 2019.
- [12] X. Chen and N. Li, “Leveraging two-stage adaptive robust optimization for power flexibility aggregation,” *IEEE Transactions on Smart Grid*, vol. 12, no. 5, pp. 3954–3965, 2021.
- [13] F. L. Müller, J. Szabó, O. Sundström, and J. Lygeros, “Aggregation and disaggregation of energetic flexibility from distributed energy resources,” *IEEE Transactions on Smart Grid*, vol. 10, no. 2, pp. 1205–1214, 2017.
- [14] F. Al Taha, T. Vincent, and E. Bitar, “An efficient method for quantifying the aggregate flexibility of plug-in electric vehicle populations,” *IEEE Transactions on Smart Grid*, vol. 16, no. 4, pp. 3142–3154, 2024.
- [15] E. Öztürk, T. Faulwasser, K. Worthmann, M. Preißinger, and K. Rheinberger, “Alleviating the curse of dimensionality in minkowski sum approximations of storage flexibility,” *IEEE Transactions on Smart Grid*, vol. 15, no. 6, pp. 5733–5743, 2024.
- [16] W. Lin, Y. Wang, J. Wu, and F. Feng, “Model-free aggregation for virtual power plants using input convex neural networks,” *IEEE Transactions on Smart Grid*, vol. 16, no. 3, pp. 2404–2415, 2025.
- [17] S. Taheri, V. Kekatos, S. Veeramachaneni, and B. Zhang, “Data-driven modeling of aggregate flexibility under uncertain and non-convex device models,” *IEEE Transactions on Smart Grid*, vol. 13, no. 6, pp. 4572–4582, 2022.
- [18] K. Hreinsson, A. Scaglione, M. Alizadeh, and Y. Chen, “New insights from the shapley-folkman lemma on dispatchable demand in energy markets,” *IEEE Transactions on Power Systems*, vol. 36, no. 5, pp. 4028–4041, 2021.
- [19] W. Han and Y. Yang, “Statistical inference in mean-field variational bayes,” *arXiv preprint arXiv:1911.01525*, 2019.
- [20] X. Guo, A. Hu, R. Xu, and J. Zhang, “Learning mean-field games,” *Advances in neural information processing systems*, vol. 32, 2019.
- [21] M. Mehrabi, O. Karaduman, and S. Wager, “Optimal mechanisms for demand response: An indifference set approach,” *arXiv preprint arXiv:2409.07655*, 2024.
- [22] M. Yi, S. Alghumayjan, and B. Xu, “Perturbed decision-focused learning for modeling strategic energy storage,” *IEEE Transactions on Smart Grid*, 2025.
- [23] I. Molchanov, *Theory of random sets*. Springer, 2005.
- [24] R. J. Aumann, “Integrals of set-valued functions,” *Journal of mathematical analysis and applications*, vol. 12, no. 1, pp. 1–12, 1965.
- [25] Z. Artstein and R. A. Vitale, “A strong law of large numbers for random compact sets,” *The Annals of Probability*, pp. 879–882, 1975.
- [26] R. M. Starr, “Quasi-equilibria in markets with non-convex preferences,” *Econometrica: journal of the Econometric Society*, pp. 25–38, 1969.
- [27] “IKEA Germany launches dynamic electricity tariff,” [Online]. Available: <https://bit.ly/49B3Vxk> (accessed Jan. 23, 2026), January 2026.
- [28] C. Chen, S. Bose, T. D. Mount, and L. Tong, “Wholesale market participation of DERAs: DSO-DERA-ISO coordination,” *IEEE Transactions on Power Systems*, vol. 39, no. 5, pp. 6605–6614, 2024.
- [29] B. Amos and J. Z. Kolter, “Optnet: Differentiable optimization as a layer in neural networks,” in *International conference on machine learning*. PMLR, 2017, pp. 136–145.
- [30] A. Agrawal, B. Amos, S. Barratt, S. Boyd, S. Diamond, and J. Z. Kolter, “Differentiable convex optimization layers,” *Advances in neural information processing systems*, vol. 32, 2019.
- [31] “Dataset of electricity prices,” [Online]. Available: <https://bit.ly/4r4w4mg> (accessed Sep. 27, 2025), September 2025.

TABLE II: Random variables versus random sets.

Concept	Random variable \mathbf{x}	Random set \mathcal{X}
Object (value space)	$\mathbf{x} : \Omega \rightarrow \mathbb{R}^n$, a measurable map taking values in \mathbb{R}^n	$\mathcal{X} : \Omega \rightarrow 2^{\mathbb{R}^n}$, a measurable map taking values in nonempty, compact subsets of \mathbb{R}^n (Definition 1)
Realization	For a fixed outcome ω in the probability space Ω , $\mathbf{x}(\omega) \in \mathbb{R}^n$ is a single point	For a fixed outcome ω in the probability space Ω , $\mathcal{X}(\omega) \subset \mathbb{R}^n$ is a single set
Addition / aggregation	Algebraic sum: $\sum_{i=1}^I \mathbf{x}_i$	Minkowski sum (set addition): $\bigoplus_{i=1}^I \mathcal{X}_i$
Sample mean	Mean-field variable: $\bar{\mathbf{x}}_I := \frac{1}{I} \sum_{i=1}^I \mathbf{x}_i$	Mean-field set: $\bar{\mathcal{X}}_I := \frac{1}{I} \bigoplus_{i=1}^I \mathcal{X}_i$
Expectation	Expected value: $\mathbb{E}[\mathbf{x}]$	Aumann expectation: $\mathbb{E}[\mathcal{X}] := \{ \mathbb{E}[\mathbf{x}] \mid \mathbf{x} \text{ is a selection of } \mathcal{X} \}$, often equivalent to $\mathbb{E}[\text{Conv}(\mathcal{X})]$ (Lemma 1)
Distance measure	Norm difference: $\ \bar{\mathbf{x}}_I - \mathbb{E}[\mathbf{x}]\ $	Hausdorff distance: $d_H(\bar{\mathcal{X}}_I, \mathbb{E}[\text{Conv}(\mathcal{X})])$
Strong law of large numbers	$\bar{\mathbf{x}}_I \xrightarrow[I \rightarrow \infty]{\text{a.s.}} \mathbb{E}[\mathbf{x}]$	$d_H(\bar{\mathcal{X}}_I, \mathbb{E}[\text{Conv}(\mathcal{X})]) \xrightarrow[I \rightarrow \infty]{\text{a.s.}} 0$ (Lemma 1)

VII. APPENDIX

A. Comparison of Random Variables and Random Sets

This appendix provides an informal comparison between random variables and random sets. Our goal is to highlight that familiar notions for random variables—such as expectation, sample means, and the law of large numbers—admit natural counterparts for random sets, which underpin the mean-field analysis in Section III-A. Throughout, we work on a non-atomic probability space and assume the random set is integrable.

1) *Side-by-side comparison.* Table II summarizes the key correspondences between random variables and random sets that are directly used in our mean-field analysis. In particular, aggregation is captured by Minkowski addition, and convergence is measured via the Hausdorff distance.

These correspondences enable a random-set analog of the strong law of large numbers. Specifically, Lemma 1 shows that the empirical mean-field set (construction via Minkowski averaging) converges almost surely to a deterministic limit, thereby justifying our use of a deterministic mean-field limit to represent the aggregate flexibility of a large storage population.

2) *From points to sets.* The key distinction is that a random variable realizes a *point* in \mathbb{R}^n , whereas a random set realizes a *compact set* in \mathbb{R}^n for each outcome ω . Accordingly, the appropriate notion of expectation is the Aumann expectation, defined through (measurable) selections of the random set. Lemma 1 further implies that Minkowski averaging of random sets leads, in the large-population limit, to the Aumann expectation of the convexified set $\text{Conv}(\mathcal{X})$ under Hausdorff convergence. This is the precise sense in which random-set aggregation mirrors the classical sample-mean convergence

for random variables, while yielding a tractable deterministic limit suitable for population-level modeling.

3) *A toy example.* To illustrate the analogy, consider a one-dimensional example. Let ξ be a nonnegative integrable random variable and define the random set

$$\mathcal{X}(\omega) := [0, \xi(\omega)] = \{x \in \mathbb{R} \mid 0 \leq x \leq \xi(\omega)\}.$$

A single realization of \mathcal{X} is thus an interval $[0, \xi(\omega)]$.

Now consider I i.i.d. random sets $\{\mathcal{X}_i\}_{i=1}^I$, where $\mathcal{X}_i = [0, \xi_i]$ and $\{\xi_i\}_{i=1}^I$ are i.i.d. random variables. The mean-field Minkowski sum becomes

$$\frac{1}{I} \bigoplus_{i=1}^I \mathcal{X}_i = \left[0, \frac{1}{I} \sum_{i=1}^I \xi_i \right].$$

By the standard strong law of large numbers for random variables, $\frac{1}{I} \sum_{i=1}^I \xi_i \rightarrow \mathbb{E}[\xi_i]$ almost surely as $I \rightarrow \infty$. Hence, in Hausdorff distance,

$$\lim_{I \rightarrow \infty} d_H \left(\frac{1}{I} \bigoplus_{i=1}^I \mathcal{X}_i, [0, \mathbb{E}[\xi_i]] \right) =_{\text{a.s.}} 0.$$

In this example, Lemma 1 reduces exactly to this statement with $\mathcal{X}_i = [0, \xi_i]$ and $\mathbb{E}[\text{Conv}(\mathcal{X}_i)] = [0, \mathbb{E}[\xi_i]]$. This example shows how the law of large numbers for random sets generalizes the classical law of large numbers for random variables.

B. Proof of Proposition 1

1) *Aggregate flexibility set.* Under Assumption 1, the augmented sets $\{\tilde{\mathcal{P}}_i^E\}_{i=1}^I$ are integrable i.i.d. random sets defined on a non-atomic probability space. Projecting $\{\tilde{\mathcal{P}}_i^E\}_{i=1}^I$ onto the power coordinates shows that the flexibility sets $\{\mathcal{P}_i^E\}_{i=1}^I$

are also integrable i.i.d. random sets defined on a non-atomic probability space. Therefore, Lemma 1 applies and gives

$$\lim_{I \rightarrow \infty} d_H(\mathcal{P}_I^M, \mathbb{E}[\text{Conv}(\mathcal{P}_i^E)]) =_{\text{a.s.}} 0.$$

That is, \mathcal{P}_I^M defined in (5) converges almost surely in the Hausdorff distance to a nonempty, compact, and convex set

$$\lim_{I \rightarrow \infty} \mathcal{P}_I^M =_{\text{a.s.}} \mathcal{P}^L, \quad \mathcal{P}^L = \mathbb{E}[\text{Conv}(\mathcal{P}_i^E)].$$

2) *Augmented power-cost set.* Define the mean-field augmented set by

$$\widetilde{\mathcal{P}}_I^M := \frac{1}{I} \bigoplus_{i=1}^I \widetilde{\mathcal{P}}_i^E \subset \mathbb{R}^{2T+1}.$$

Applying Lemma 1 to $\{\widetilde{\mathcal{P}}_i^E\}_{i=1}^I$ yields

$$\lim_{I \rightarrow \infty} d_H(\widetilde{\mathcal{P}}_I^M, \mathbb{E}[\text{Conv}(\widetilde{\mathcal{P}}_i^E)]) =_{\text{a.s.}} 0.$$

3) *Identification of the cost limit.* From the definition of C_I^M in (6) and of the augmented sets in Section III-B, one verifies that the truncated epigraph of the mean-field aggregate cost coincides with the mean-field augmented set, i.e., $\text{epi } C_I^M = \widetilde{\mathcal{P}}_I^M$. Combining this identity with the convergence in Step 2, we obtain

$$\lim_{I \rightarrow \infty} d_H(\text{epi } C_I^M, \mathbb{E}[\text{Conv}(\widetilde{\mathcal{P}}_i^E)]) =_{\text{a.s.}} 0.$$

The limit set $\mathbb{E}[\text{Conv}(\widetilde{\mathcal{P}}_i^E)]$ is nonempty, compact, and convex, and it is upward closed within the truncation level in the cost coordinate. Hence it is the truncated epigraph of a unique convex, continuous, bounded function $C^L(\mathbf{p})$ defined on its projection onto the power space, which equals \mathcal{P}^L . In other words,

$$\text{epi } C^L(\mathbf{p}) = \mathbb{E}[\text{Conv}(\widetilde{\mathcal{P}}_i^E)].$$

By standard results on epigraph convergence, the Hausdorff convergence of the truncated epigraphs implies that C_I^M epi-converges to C^L . Since C^L is continuous on \mathcal{P}^L , it follows that, for all $\mathbf{p} \in \mathcal{P}^L$,

$$\lim_{I \rightarrow \infty} C_I^M(\mathbf{p}) =_{\text{a.s.}} C^L(\mathbf{p}).$$

Finally, for each device,

$$C_i^E(\mathbf{p}_i) = \boldsymbol{\lambda}^\top (\mathbf{p}_i^C - \mathbf{p}_i^D) + U_i^E(\mathbf{p}_i),$$

so for any aggregate profile \mathbf{p} we can write

$$C_I^M(\mathbf{p}) = \boldsymbol{\lambda}^\top (\mathbf{p}^C - \mathbf{p}^D) + U_I^M(\mathbf{p}),$$

for an aggregate disutility according to (6)

$$U_I^M(\mathbf{p}) := \inf_{\{\mathbf{p}_i\}_{i=1}^I} \left\{ \frac{1}{I} \sum_{i=1}^I U_i^E(\mathbf{p}_i) \mid \mathbf{p} = \frac{1}{I} \sum_{i=1}^I \mathbf{p}_i, \mathbf{p}_i \in \mathcal{P}_i^E \right\}.$$

Taking limits in I for equation $C_I^M(\mathbf{p}) = \boldsymbol{\lambda}^\top (\mathbf{p}^C - \mathbf{p}^D) + U_I^M(\mathbf{p})$, we obtain the stated decomposition

$$C^L(\mathbf{p}) = \boldsymbol{\lambda}^\top (\mathbf{p}^C - \mathbf{p}^D) + U^L(\mathbf{p}),$$

where

$$\lim_{I \rightarrow \infty} U_I^M(\mathbf{p}) =_{\text{a.s.}} U^L(\mathbf{p}).$$

The term $\boldsymbol{\lambda}^\top (\mathbf{p}^C - \mathbf{p}^D)$ is linear on \mathbb{R}^{2T} , and, as shown above, C^L is continuous, convex, and bounded on \mathcal{P}^L . Hence U^L , being the difference between C^L and a linear function, is also convex, continuous, and bounded on \mathcal{P}^L . \square

C. Proof of Proposition 2

1) *Augmented-point error bound.* For each price vector $\boldsymbol{\pi}_d$, $d = 1, \dots, D$, define the augmented points

$$\mathbf{z}_A^*(\boldsymbol{\pi}_d) := [\mathbf{p}_d^{*\top}, u_d^*]^\top, \quad \mathbf{z}_B^*(\boldsymbol{\pi}_d) := [\widehat{\mathbf{p}}_d^{*\top}, \widehat{u}_d^*]^\top,$$

and set

$$e_d := \|\mathbf{z}_A^*(\boldsymbol{\pi}_d) - \mathbf{z}_B^*(\boldsymbol{\pi}_d)\|.$$

By definition of e_d , this gives, for all $d = 1, \dots, D$,

$$e_d^2 = \|\mathbf{p}_d^* - \widehat{\mathbf{p}}_d^*\|^2 + |u_d^* - \widehat{u}_d^*|^2. \quad (19)$$

2) *Support function bound.* For a nonempty compact set $S \subset \mathbb{R}^{2T+1}$, its support function is

$$\delta(\mathbf{x}; S) := \sup_{\mathbf{z} \in S} \mathbf{x}^\top \mathbf{z}, \quad \mathbf{x} \in \mathbb{R}^{2T+1}.$$

A standard argument (evaluating at a maximizer for $\delta(\mathbf{y}; S)$ and applying the Cauchy-Schwarz inequality) shows that

$$|\delta(\mathbf{x}; S) - \delta(\mathbf{y}; S)| \leq \left(\sup_{\mathbf{z} \in S} \|\mathbf{z}\| \right) \|\mathbf{x} - \mathbf{y}\| \quad \forall \mathbf{x}, \mathbf{y} \in \mathbb{R}^{2T+1}. \quad (20)$$

By definition of R , $\|\mathbf{z}\| \leq R$ for all $\mathbf{z} \in \mathcal{A} \cup \mathcal{B}$, so $\sup_{\mathbf{z} \in \mathcal{A}} \|\mathbf{z}\| \leq R$ and $\sup_{\mathbf{z} \in \mathcal{B}} \|\mathbf{z}\| \leq R$.

For each d , define the normalized price direction

$$\hat{\boldsymbol{\pi}}_d := \boldsymbol{\pi}_d / \|\boldsymbol{\pi}_d\|.$$

Fix any unit vector \mathbf{w} with $\|\mathbf{w}\| = 1$. By the definition of $\rho(\Pi)$ in (11), there exists $d^* \in \{1, \dots, D\}$ such that

$$\|\mathbf{w} - \hat{\boldsymbol{\pi}}_{d^*}\| \leq \rho(\Pi).$$

Hence,

$$\|(-\mathbf{w}) - (-\hat{\boldsymbol{\pi}}_{d^*})\| = \|\mathbf{w} - \hat{\boldsymbol{\pi}}_{d^*}\| \leq \rho(\Pi).$$

Insert and subtract $\delta(-\hat{\boldsymbol{\pi}}_{d^*}; \mathcal{A})$ and $\delta(-\hat{\boldsymbol{\pi}}_{d^*}; \mathcal{B})$, and apply the triangle inequality:

$$\begin{aligned} |\delta(-\mathbf{w}; \mathcal{A}) - \delta(-\mathbf{w}; \mathcal{B})| &\leq |\delta(-\mathbf{w}; \mathcal{A}) - \delta(-\hat{\boldsymbol{\pi}}_{d^*}; \mathcal{A})| \\ &\quad + |\delta(-\hat{\boldsymbol{\pi}}_{d^*}; \mathcal{A}) - \delta(-\hat{\boldsymbol{\pi}}_{d^*}; \mathcal{B})| \\ &\quad + |\delta(-\hat{\boldsymbol{\pi}}_{d^*}; \mathcal{B}) - \delta(-\mathbf{w}; \mathcal{B})|. \end{aligned} \quad (21)$$

By (20) and $\|\mathbf{z}\| \leq R$ on \mathcal{A} and \mathcal{B} , the first and third terms satisfy

$$|\delta(-\mathbf{w}; \mathcal{A}) - \delta(-\hat{\boldsymbol{\pi}}_{d^*}; \mathcal{A})| \leq R \rho(\Pi),$$

$$|\delta(-\hat{\boldsymbol{\pi}}_{d^*}; \mathcal{B}) - \delta(-\mathbf{w}; \mathcal{B})| \leq R \rho(\Pi).$$

Scaling does not change the optimizer, so $z_{\mathcal{A}}^*(\pi_{d^*})$ and $z_{\mathcal{B}}^*(\pi_{d^*})$ are also optimal for the normalized direction $\hat{\pi}_{d^*}$. Thus

$$\delta(-\hat{\pi}_{d^*}; \mathcal{A}) = -\hat{\pi}_{d^*}^\top z_{\mathcal{A}}^*(\pi_{d^*}), \quad \delta(-\hat{\pi}_{d^*}; \mathcal{B}) = -\hat{\pi}_{d^*}^\top z_{\mathcal{B}}^*(\pi_{d^*}),$$

and

$$\begin{aligned} |\delta(-\hat{\pi}_{d^*}; \mathcal{A}) - \delta(-\hat{\pi}_{d^*}; \mathcal{B})| &= |\hat{\pi}_{d^*}^\top (z_{\mathcal{A}}^*(\pi_{d^*}) - z_{\mathcal{B}}^*(\pi_{d^*}))| \\ &\leq \|\hat{\pi}_{d^*}\| \|z_{\mathcal{A}}^*(\pi_{d^*}) - z_{\mathcal{B}}^*(\pi_{d^*})\| \\ &= \|z_{\mathcal{A}}^*(\pi_{d^*}) - z_{\mathcal{B}}^*(\pi_{d^*})\| \\ &= e_{d^*}, \end{aligned}$$

where the inequality is by Cauchy-Schwarz. Moreover, $e_{d^*} \leq \max_d e_d \leq \sqrt{\sum_{d=1}^D e_d^2}$. Substituting these bounds into (21) yields, for every $\|\mathbf{w}\| = 1$,

$$|\delta(-\mathbf{w}; \mathcal{A}) - \delta(-\mathbf{w}; \mathcal{B})| \leq \sqrt{\sum_{d=1}^D e_d^2} + 2R\rho(\Pi).$$

The same bound holds with \mathbf{w} in place of $-\mathbf{w}$, so

$$|\delta(\mathbf{w}; \mathcal{A}) - \delta(\mathbf{w}; \mathcal{B})| \leq \sqrt{\sum_{d=1}^D e_d^2} + 2R\rho(\Pi), \quad \forall \|\mathbf{w}\| = 1.$$

3) *Hausdorff distance bound.* For nonempty compact convex sets, the Hausdorff distance satisfies

$$d_H(\mathcal{A}, \mathcal{B}) = \sup_{\|\mathbf{w}\|=1} |\delta(\mathbf{w}; \mathcal{A}) - \delta(\mathbf{w}; \mathcal{B})|.$$

Taking the supremum over $\|\mathbf{w}\| = 1$ in the previous inequality gives

$$d_H(\mathcal{A}, \mathcal{B}) \leq \sqrt{\sum_{d=1}^D e_d^2} + 2R\rho(\Pi),$$

which is the desired bound stated in Proposition 2. \square

D. Proof of Proposition 3

Fix any day d . For notational simplicity, we suppress the subscript d throughout the proof.

1) *Augmented sets.* For each device i , define

$$\bar{\mathcal{P}}_i^E := \left\{ [\mathbf{p}_i^\top, u_i]^\top \mid \mathbf{p}_i \in \mathcal{P}_i^E, [\mathbf{p}_i^\top, u_i]^\top \in \text{epi } U_i^E \right\} \subset \mathbb{R}^{2T+1}.$$

By the similar derivation as in Section VII-B, the family $\{\bar{\mathcal{P}}_i^E\}_{i=1}^I$ consists of integrable i.i.d. random sets.

Given λ , the corresponding augmented price vector is

$$\pi := [\lambda^\top, -\lambda^\top, 1]^\top.$$

For any nonempty set $\mathcal{X} \subset \mathbb{R}^{2T+1}$, define the value function

$$h(\pi; \mathcal{X}) := \min_{[\mathbf{p}^\top, u]^\top \in \mathcal{X}} \pi^\top [\mathbf{p}^\top, u]^\top.$$

In particular,

$$h(\pi; \bar{\mathcal{P}}_i^E) := \min_{[\mathbf{p}_i^\top, u_i]^\top \in \bar{\mathcal{P}}_i^E} \pi^\top [\mathbf{p}_i^\top, u_i]^\top.$$

Because the objective is increasing in u_i , there always exists an optimal solution with $u_i = U_i^E(\mathbf{p}_i)$. Hence

$$h(\pi; \bar{\mathcal{P}}_i^E) = \min_{\mathbf{p}_i \in \mathcal{P}_i^E} [\lambda^\top (\mathbf{p}_i^C - \mathbf{p}_i^D) + U_i^E(\mathbf{p}_i)] = \min_{\mathbf{p}_i \in \mathcal{P}_i^E} C_i^E(\mathbf{p}_i).$$

2) *Value connection.* Recall the support function

$$\delta(\pi; \mathcal{X}) := \sup_{\mathbf{x} \in \mathcal{X}} \pi^\top \mathbf{x}.$$

For any nonempty set \mathcal{X} , we have

$$h(\pi; \mathcal{X}) = \min_{\mathbf{x} \in \mathcal{X}} \pi^\top \mathbf{x} = -\sup_{\mathbf{x} \in \mathcal{X}} (-\pi)^\top \mathbf{x} = -\delta(-\pi; \mathcal{X}).$$

We recall two standard facts [23]: (i) for any nonempty set \mathcal{X} , $\delta(\pi; \mathcal{X}) = \delta(\pi; \text{Conv}(\mathcal{X}))$; (ii) for random compact convex sets we have

$$\mathbb{E}[\delta(\pi; \mathcal{X})] = \delta(\pi; \mathbb{E}[\mathcal{X}])$$

and $\mathbb{E}[\mathcal{X}]$ is the Aumann expectation as explained in Definition 2.

Then, we have

$$\begin{aligned} \mathbb{E}[\delta(-\pi; \bar{\mathcal{P}}_i^E)] &\stackrel{(i)}{=} \mathbb{E}[\delta(-\pi; \text{Conv}(\bar{\mathcal{P}}_i^E))] \\ &\stackrel{(ii)}{=} \delta(-\pi; \mathbb{E}[\text{Conv}(\bar{\mathcal{P}}_i^E)]). \end{aligned}$$

Using $h(\pi; \mathcal{X}) = -\delta(-\pi; \mathcal{X})$, we obtain

$$\min_{[\mathbf{p}^\top, u]^\top \in \mathbb{E}[\text{Conv}(\bar{\mathcal{P}}_i^E)]} \pi^\top [\mathbf{p}^\top, u]^\top = \mathbb{E}[h(\pi; \bar{\mathcal{P}}_i^E)].$$

For each random set $\bar{\mathcal{P}}_i^E$, choose an optimal solution $[\mathbf{p}_i^{*\top}, u_i^*]^\top$ of $h(\pi; \bar{\mathcal{P}}_i^E)$ with $u_i^* = U_i^E(\mathbf{p}_i^*)$. Then $[\mathbf{p}_i^{*\top}, u_i^*]^\top$ is a measurable selection [‡] of the random set $\bar{\mathcal{P}}_i^E$, and

$$\mathbb{E}[h(\pi; \bar{\mathcal{P}}_i^E)] = \mathbb{E}[\pi^\top [\mathbf{p}_i^{*\top}, u_i^*]^\top] = \pi^\top \mathbb{E}[[\mathbf{p}_i^{*\top}, u_i^*]^\top].$$

By the definition of the Aumann expectation, the point

$$\mathbb{E}[[\mathbf{p}_i^{*\top}, u_i^*]^\top] \in \mathbb{E}[\text{Conv}(\bar{\mathcal{P}}_i^E)]$$

attains the minimum above.

3) *Equality of minimizers.* By Proposition 1 and the linear relation between the cost and disutility truncated epigraphs, we have

$$\mathbb{E}[\text{Conv}(\bar{\mathcal{P}}_i^E)] = \text{epi } U^L,$$

so minimizing $\pi^\top [\mathbf{p}^\top, u]^\top$ over $\mathbb{E}[\text{Conv}(\bar{\mathcal{P}}_i^E)]$ is equivalent to the mean-field problem

$$\min_{\mathbf{p} \in \mathcal{P}^L} \{ \lambda^\top (\mathbf{p}^C - \mathbf{p}^D) + U^L(\mathbf{p}) \}.$$

In Step 2) above, we show that $\mathbb{E}[[\mathbf{p}_i^{*\top}, u_i^*]^\top]$ is a minimizer of $\pi^\top [\mathbf{p}^\top, u]^\top$ over $\mathbb{E}[\text{Conv}(\bar{\mathcal{P}}_i^E)]$. Therefore its first and second components,

$$\mathbf{p}^* := \mathbb{E}[\mathbf{p}_i^*], \quad u^* := \mathbb{E}[u_i^*],$$

[‡]The definition of selection is explained in Definition 2.

define a mean-field optimal response $[\mathbf{p}^{*\top}, u^*]^\top$ for the price vector $\boldsymbol{\lambda}$.

4) *Law of large numbers.* For the fixed day (with indices suppressed), let

$$\mathbf{z}_i^* := [\mathbf{p}_i^{*\top}, u_i^*]^\top$$

denote the optimal response of device i under the price $\boldsymbol{\lambda}$. By the i.i.d. structure of the devices, the vectors \mathbf{z}_i^* are i.i.d. with finite norm and satisfy

$$\mathbb{E}[\mathbf{z}_i^*] = [\mathbf{p}^{*\top}, u^*]^\top,$$

thanks to the boundedness assumptions in Section III-B. Hence the strong law of large numbers yields

$$\frac{1}{I} \sum_{i=1}^I \mathbf{z}_i^* \xrightarrow[I \rightarrow \infty]{\text{a.s.}} \mathbb{E}[\mathbf{z}_i^*] = [\mathbf{p}^{*\top}, u^*]^\top.$$

Taking the first and second components gives

$$\lim_{I \rightarrow \infty} \frac{1}{I} \sum_{i=1}^I \mathbf{p}_i^* =_{\text{a.s.}} \mathbf{p}^*, \quad \lim_{I \rightarrow \infty} \frac{1}{I} \sum_{i=1}^I u_i^* =_{\text{a.s.}} u^*.$$

Finally, since the day d was arbitrary, the same argument applies to every $d = 1, \dots, D$. Restoring the subscript d yields

$$\lim_{I \rightarrow \infty} \frac{1}{I} \sum_{i=1}^I \mathbf{p}_{i,d}^* =_{\text{a.s.}} \mathbf{p}_d^*, \quad \lim_{I \rightarrow \infty} \frac{1}{I} \sum_{i=1}^I u_{i,d}^* =_{\text{a.s.}} u_d^*.$$

which is precisely the statement of Proposition 3. \square

E. Gradient Derivation and Algorithm Procedure

1) *Gradient Derivation.* We first rewrite the inner-level problem (18) in standard form with inequality constraints $g(\mathbf{z}_\mathcal{B}(\boldsymbol{\pi}_d), \Theta) \leq \mathbf{0}$. Its Lagrangian is

$$\mathcal{L}(\mathbf{z}_\mathcal{B}(\boldsymbol{\pi}_d), \boldsymbol{\mu}; \Theta) = \boldsymbol{\pi}_d^\top \mathbf{z}_\mathcal{B}(\boldsymbol{\pi}_d) + \boldsymbol{\mu}^\top g(\mathbf{z}_\mathcal{B}(\boldsymbol{\pi}_d), \Theta),$$

where $\boldsymbol{\mu} \geq \mathbf{0}$ is the vector of Lagrange multipliers.

By convexity, the KKT conditions are necessary and sufficient for optimality. Hence, at an optimum $(\mathbf{z}_\mathcal{B}^*(\boldsymbol{\pi}_d), \boldsymbol{\mu}^*)$, we have

$$\mathcal{K}(\mathbf{z}_\mathcal{B}^*(\boldsymbol{\pi}_d), \boldsymbol{\mu}^*; \Theta) = \begin{bmatrix} \nabla_{\mathbf{z}} \mathcal{L}(\mathbf{z}_\mathcal{B}^*(\boldsymbol{\pi}_d), \boldsymbol{\mu}^*; \Theta) \\ \boldsymbol{\mu}^* \odot g(\mathbf{z}_\mathcal{B}^*(\boldsymbol{\pi}_d), \Theta) \end{bmatrix} = \mathbf{0},$$

where \odot denotes elementwise multiplication and \mathcal{K} collects the stationarity and complementarity conditions.

Under standard regularity conditions for differentiable optimization layers [29], [30], the solution mapping is differentiable with respect to Θ . Let $\mathbf{y} := [\mathbf{z}_\mathcal{B}^{*\top}(\boldsymbol{\pi}_d), \boldsymbol{\mu}^{*\top}]^\top$. Differentiating $\mathcal{K}(\mathbf{y}; \Theta) = \mathbf{0}$ with respect to Θ yields

$$\frac{\partial \mathcal{K}}{\partial \Theta} + \frac{\partial \mathcal{K}}{\partial \mathbf{y}} \frac{\partial \mathbf{y}}{\partial \Theta} = \mathbf{0},$$

which leads to

$$\frac{\partial \mathbf{y}}{\partial \Theta} = - \left[\frac{\partial \mathcal{K}}{\partial \mathbf{y}} \right]^{-1} \frac{\partial \mathcal{K}}{\partial \Theta}. \quad (22)$$

The sensitivity $\partial \mathbf{z}_\mathcal{B}^*(\boldsymbol{\pi}_d) / \partial \Theta$ is given by the block of $\partial \mathbf{y} / \partial \Theta$ associated with $\mathbf{z}_\mathcal{B}^*(\boldsymbol{\pi}_d)$.

2) *Algorithm Procedure.* The solution algorithm is summarized as follows.

Initialization: Collect historical price-response pairs $(\boldsymbol{\pi}_d, \mathbf{z}_\mathcal{A}^*(\boldsymbol{\pi}_d))$, $d = 1, \dots, D$. Initialize the surrogate parameters $\Theta^{(0)}$, choose a maximum number of iterations O , and set $o = 0$.

Step I: For the current parameters $\Theta^{(o)}$, solve (18) for each $d = 1, \dots, D$ to obtain $\mathbf{z}_\mathcal{B}^{*(o)}(\boldsymbol{\pi}_d)$.

Step II: Evaluate the loss $F(\Theta^{(o)})$ according to (16).

Step III: Compute $\partial \mathbf{z}_\mathcal{B}^{*(o)}(\boldsymbol{\pi}_d) / \partial \Theta^{(o)}$ via (22), and then compute $\nabla_\Theta F(\Theta^{(o)})$ using the chain rule as in (17).

Step IV: Update the parameters using (17) to obtain $\Theta^{(o+1)}$. If $o < O - 1$, set $o \leftarrow o + 1$ and return to *Step I*; otherwise, terminate and output $\Theta^{(O)}$.

This procedure requires solving the convex programs (18) at each iteration, which can be efficiently handled by off-the-shelf convex optimization solvers.

F. Model Details

We use the Adam optimizer in PyTorch with a learning rate of 0.01 for all experiments. Baseline models are configured as follows:

- **MLP:** four layers with 48 hidden neurons. The input is the electricity price vector, and the output is the aggregate power profile.
- **LSTM:** four LSTM layers with one fully-connected layer.
- **SVR:** trained as 24 independent models. Each model receives the same 24-hour price vector and predicts the aggregate power for its corresponding hour.

where \odot denotes elementwise multiplication and \mathcal{K} collects the stationarity and complementarity conditions.

Under standard regularity conditions for differentiable optimization layers [29], [30], the solution mapping is differentiable with respect to Θ . Let $\mathbf{y} := [\mathbf{z}_\mathcal{B}^{*\top}(\boldsymbol{\pi}_d), \boldsymbol{\mu}^{*\top}]^\top$. Differentiating $\mathcal{K}(\mathbf{y}; \Theta) = \mathbf{0}$ with respect to Θ yields

$$\frac{\partial \mathcal{K}}{\partial \Theta} + \frac{\partial \mathcal{K}}{\partial \mathbf{y}} \frac{\partial \mathbf{y}}{\partial \Theta} = \mathbf{0},$$

which leads to

$$\frac{\partial \mathbf{y}}{\partial \Theta} = - \left[\frac{\partial \mathcal{K}}{\partial \mathbf{y}} \right]^{-1} \frac{\partial \mathcal{K}}{\partial \Theta}. \quad (22)$$